IEEE Access
Multidisciplinary | Rapid Review | Open Access Journal

Received December 9, 2019, accepted December 30, 2019, date of publication January 9, 2020, date of current version January 17, 2020.

Digital Object Identifier 10.1109/ACCESS.2020.2965215

An Approach to Improve System Performance in the Vehicle-Grid System Using Sliding Mode Control Under Multiple Operation Conditions

YUTING ZHANG, SIQI WU, (Student Member, IEEE), ZHIGANG LIU, (Senior Member, IEEE), QIXIANG YAN, AND TAO CHEN

School of Electrical Engineering, Southwest Jiaotong University, Chengdu 610031, China

Corresponding author: Zhigang Liu (liuzg_cd@126.com)

This work was supported in part by the National Nature Science Foundation of China under Grant U1434203.

ABSTRACT To improve the performance of vehicle-grid system under multiple operation conditions and suppress the low-frequency oscillation (LFO) in electrified railways, this paper proposed a control strategy of electric multiple units (EMUs) traction line-side converter (LSC) based on sliding mode control (SMC). First, the accurate model of EMUs is established and then the mathematical model of it in the *d-q* frame is derived. Then, the application of sliding mode variable structure control strategy in the LSC of EMUs is presented in detail, which includes the design of outer loop voltage sliding mode surface and inner loop current control law. Moreover, the control performance for EMUs based on SMC and traditional linear proportional integral (PI) control is compared under multiple operation conditions in the case of one traction drive unit of EMUs and multi-EMUs, respectively. Finally, experiments are implemented on the hardware in the loop simulation platform based on software StarSim. The experiments results show that, compared with PI control, SMC owns better control performance, such as the lower total harmonic distortion of traction line-side current under multiple conditions, lower voltage fluctuation when braking occurs, better anti-interference ability with the change of system parameters, and can effectively suppress the LFO occurs under operation mode.

INDEX TERMS Electrified railways, multiple operation conditions, sliding mode control, total harmonic distortion, vehicle-grid system.

I. INTRODUCTION

In recent years, high-speed railways have developed rapidly, and the alternating current-direct current-alternating current (AC-DC-AC) trains have been vigorously developed. AC-DC-AC trains have the characteristics of low harmonic content on the grid side and high power factor, so they are widely used in railways [1]. For the electric multiple units (EMUs), the low-order harmonics in the grid-side current are mainly odd harmonics, such as the 3^{rd}, 5^{th}, 7^{th} and 9^{th} harmonics [2]. When EMUs are put into operation and run under the traction or braking conditions, the traction power of EMUs changes, and the total harmonic distortion (THD) of grid-side current will change accordingly. The smaller the power is, the greater the THD of grid-side current is [3]. Moreover, EMUs also have the disadvantages of large overshoot when EMUs are powered and poor system robustness. So, it is very necessary to improve the performance of the vehicle-grid system.

Nowadays, the phenomenon of low-frequency oscillation (LFO) in vehicle-grid system has attracted researchers' attention. LFO is characterized by the amplitude fluctuation of voltage, current or other electrical quantities with a synchronous oscillation frequency of 2-7 Hz [4]–[8]. It is believed that the LFO is mostly caused by the mismatch between the parameters of the traction network and the control parameters of line-side converter (LSC) [9], [10]. At present, there are many methods to suppress the LFO. In practical engineering, the simplest and easiest method is to improve the control strategies of LSC. Liu *et al.*

The associate editor coordinating the review of this manuscript and approving it for publication was Engang Tian.

proposed two kinds of control strategies of LSC based on extended state observer sliding mode control (SMC) and extended state observer model predictive control, which improved the performance of LSC and suppressed the LFO successfully [11], [12]. Geng *et al.* adopted H∞ control to obtain better dynamic and static performance and suppressed the LFO effectively [13].

The LFO usually occurs when multi-EMUs are at standstill in rail depots and rise their pantographs [14]. Although the LFO happening when the EMUs are running has not reported, some studies have pointed out the possibility of it [15]. In this situation, serious harm will be caused to EMUs and traction network and even passengers, so the researches on LFO are necessary. In [11]–[13], the inverters and the motors are all equivalent to linear resistances, since they are in inoperative states, which makes the accuracy of system model very poor. Besides, these papers only consider the LFO that occurs when multi-EMUs rise their pantographs at the same time, but do not consider that when EMUs are under operation mode.

SMC is essentially a special kind of nonlinear control. The structure of this control strategy is not fixed, but can be continuously and purposefully changed according to the current state of the system during the dynamic process, which can force the system to follow a predetermined sliding mode state trajectory. The sliding mode can be designed regardless of the systems parameters and disturbances, which indicates that SMC has the advantages of fast response, insensitivity to parameter changes and disturbances, simple physical implementation, etc. Hence, to improve the performance of vehicle-grid system under multiple operation conditions, this paper applies SMC in the control of the LSC of CRH3 EMUs.

The main contributions are presented as follows. First, the concrete model of EMUs including a twofold LSC, a DC link, a traction inverter and a traction asynchronous motor is taken into consideration. Then, the control performance of SMC under multiple operation conditions is verified by simulations and hardware in the loop (HIL) experiments. Finally, it is verified that SMC can effectively suppress the LFO occurring when EMUs run in multiple operation conditions.

This paper is organized as follows. In Section II, the *d-q* frame mathematical model of the single-phase LSC of EMUs connected to the inverter and the motor is given. In Section III, the SMC is designed for the LSC of EMUs based on the theoretical analysis. In Section IV, the simulation results of one traction drive unit of EMUs based on SMC and proportional integral (PI) control are presented and discussed in detail. The control performance based on SMC and PI control under multi-EMUs is also discussed. In Section V, the vehicle-grid system is built in the HIL simulation platform, which verifies the correctness of simulation results. Finally, the conclusions are drawn in Section VI.

II. MODEL OF ONE TRACTION DRIVE UNIT OF THE EMUs

In [16], the AC side of the inverter can be equivalent to a three-phase AC voltage source e_k $(k = 1, 2, 3)$ in series with three-phase loads R and L, as shown in Fig. 1. i_k $(k = 1, 2, 3)$ represents the three-phase equivalent current of the motor. Hence, the inverter and the motor can be equivalent to a non-constant DC voltage source in series with a resistor. Therefore, according to the substitution theorem, the load branch composed of inverter and motor can be replaced with the current source i_l, as shown in Fig. 1.

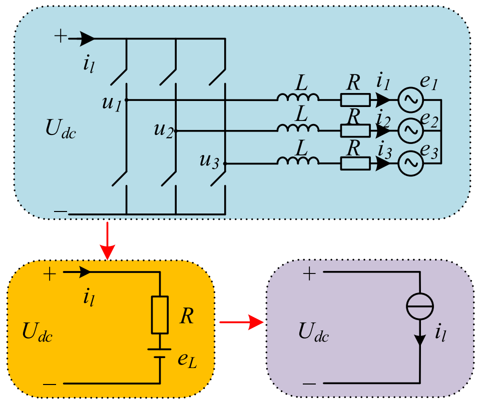

FIGURE 1. DC-side equivalent circuit of inverter.

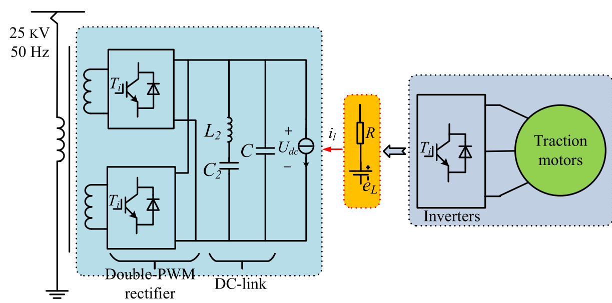

FIGURE 2. Traction drive system for basic power units of EMUs.

According to [16], i_l can be calculated as (1), where m is the pulse width modulation (PWM) ratio of the inverter; t is time; τ is the time constant of the transient component. ρ is the AC counter electromotive force amplitude factor; ω is the angular frequency; U_{dc} is the DC-side voltage. θ is the phase difference between the vector of u_k and e_k $(k = 1, 2, 3)$ and γ is the phase difference between the vector of i_k and e_k $(k = 1, 2, 3)$.

$$i_l = \frac{3m^2U_{dc}}{8}\sqrt{\frac{1+\rho^2-2\rho\cos\theta}{R^2+(\omega L)^2}} \cdot \left[\cos(\theta+\gamma) - e^{-t/\tau}\cos(\omega t+\theta+\gamma)\right] \quad (1)$$

In this paper, i_l is measured directly and output to the voltage controller of SMC, so the complicated model building process is omitted. That is to say, the application of SMC in the LSC of EMUs brings great convenience to the design of the controller.

After replacing the inverter and the motor with the current source i_l, the equivalent topological structure of one traction drive unit of EMUs can be obtained. As shown in Fig. 2, the topological structure of one traction drive unit

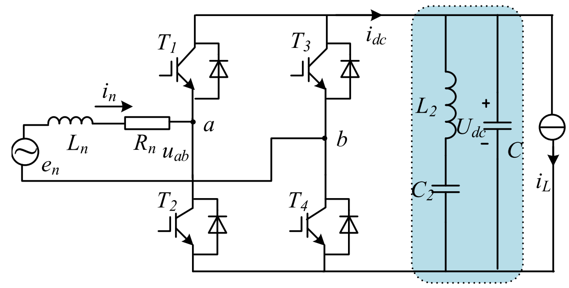

FIGURE 3. Equivalent circuit diagram of EMUs.

of CRH3 EMUs is constituted by a twofold four quadrant LSC in parallel, a DC link which consists of a secondary filter and a capacitance, a traction inverter and four traction asynchronous motors. The double-PWM rectifier and the secondary filter have the advantages of reducing system harmonics.

Fig. 3 shows the equivalent circuit diagram of EMUs. e_n is the grid-side AC voltage; i_n is the grid-side AC current; L_n and R_n are the leakage inductance and leakage resistance equivalent to the secondary side of the vehicle transformer, respectively. C is the DC-side support capacitor. u_{ab} is the voltage between note a and note b, namely the input voltage of the LSC. T_1, T_2, T_3 and T_4 are the four IGBTs of the converter.

According to the topological structure in Fig. 3, the state-space equation in (2) can be obtained.

$$\begin{cases} L_n \dfrac{di_n}{dt} = e_n - R_n i_n - u_{ab} \\ C \dfrac{dU_{dc}}{dt} = i_{dc} - i_l \end{cases} \tag{2}$$

Substituting (10) into (11), we can obtain

$$\begin{cases} L_n \dfrac{di_n}{dt} = e_n - R_n i_n - u_{ab} \\ C \dfrac{dU_{dc}}{dt} = i_{dc} - \left(\begin{aligned} & \dfrac{3m^2 U_{dc}}{8} \sqrt{\dfrac{1+\rho^2 - 2\rho\cos\theta}{R^2 + (\omega L)^2}} \\ & \cdot \left[\cos(\theta+\gamma) - e^{-t/\tau}\cos(\omega t + \theta + \gamma)\right] \end{aligned} \right) \end{cases} \tag{3}$$

Since the switching signals of the upper and lower arms of the rectifier must be reversed, the switching function is specified as follows.

$$\begin{aligned} S_a &= \begin{cases} 1, & \text{T}_1 \text{ is open} \\ 0, & \text{T}_2 \text{ is open} \end{cases} \\ S_b &= \begin{cases} 1, & \text{T}_3 \text{ is open} \\ 0, & \text{T}_4 \text{ is open} \end{cases} \end{aligned} \tag{4}$$

From Fig. 3, it can be seen that the input voltage u_{ab} has three levels: U_{dc}, 0, $-U_{dc}$. Hence, there are four types of effective switch combinations, namely $S_a S_b = 00$, 01, 10, and 11, so u_{ab} can be expressed as

$$u_{ab} = (S_a - S_b) \cdot U_{dc} \tag{5}$$

When SMC is adopted, the electrical quantity i_n which is expressed as i_α is decoupled, and a virtual AC quantity i_β is formed which owns the same amplitude and frequency as i_n with the phase delayed by 90°. Other electrical quantities can also be converted to the α-β frame in the same way. Then the electrical quantities on the d-q frame can be obtained via the Park transformation matrix in (6).

$$\begin{bmatrix} i_d \\ i_q \end{bmatrix} = \begin{bmatrix} \cos\varphi & \sin\varphi \\ -\sin\varphi & \cos\varphi \end{bmatrix} \begin{bmatrix} i_\alpha \\ i_\beta \end{bmatrix} = C_{2s/2r} \begin{bmatrix} i_\alpha \\ i_\beta \end{bmatrix} \tag{6}$$

Combining (3) and (6), the mathematical model of EMUs in the d-q rotating coordinate system is obtained as

$$\begin{cases} L_n \dfrac{di_d}{dt} = -R_n i_d + \omega L_n i_q + e_d - S_d U_{dc} \\ L_n \dfrac{di_q}{dt} = -R_n i_q - \omega L_n i_d + e_q - S_q U_{dc} \\ C \dfrac{dU_{dc}}{dt} = (S_d i_d + S_q i_q) - \dfrac{3m^2 U_{dc}}{8} \sqrt{\dfrac{1+\rho^2 - 2\rho\cos\theta}{R^2 + (\omega L)^2}} \\ \qquad \cdot \left[\cos(\theta+\gamma) - e^{-t/\tau}\cos(\omega t + \theta + \gamma)\right] \end{cases} \tag{7}$$

In (7), i_d and i_q are the decoupling components of i_n in d-q frame, e_d and e_q are the decoupling components of e_n in d-q frame, S_d and S_q are the system switching functions in d-q frame.

III. APPLICATION OF SLIDING MODE VARIABLE STRUCTURE CONTROL STRATEGY IN THE LSC OF EMUs

Ideally, when SMC is adopted, if the state point of the system runs in the area near the switching surface, it will be attracted to the area and move according to the designed sliding surface. To achieve SMC, there are two problems to be considered: the existence problem and the reachability problem. The existence condition of the sliding mode can be expressed by (8).

$$\lim_{s \to 0} s \cdot \dot{s} \leq 0 \tag{8}$$

The design of the SMC consists of two parts. The first part is the evaluation of the outer-loop voltage sliding mode surface and the second part is the selection of the inner-loop current control rate. The control goal of SMC in this paper is to stabilize the DC-side voltage of the rectifier at 3000V, and make the power factor of the grid close to 1, which means that the reactive power in grid is 0 and $i_q = 0$. The control block diagram of SMC is shown in Fig. 4.

A. OUTER LOOP VOLTAGE CONTROL

The acquisition of the sliding surface is very important for the control performance of the system. As illustrated above, the control target of this paper is U_{dc} and i_q. Therefore, U_{dc} and i_q are set as the output of the control system. Φ is the derivative of U_{dc}, which is dU_{dc}/dt. e_{udc}, e_{iq} and e_Φ respectively represent the error of U_{dc}, i_q and dU_{dc}/dt. U_{dcref}, i_{qref} and Φ_{ref} are the reference values of U_{dc}, i_q and dU_{dc}/dt,

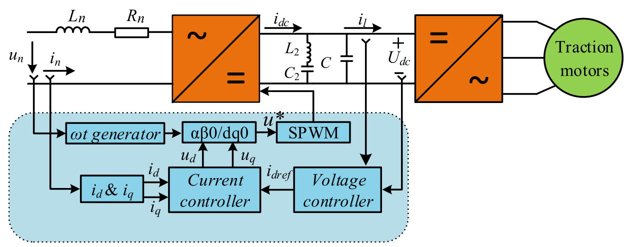

FIGURE 4. **Control block diagram of the LSC based on SMC.**

respectively. Equation (9) gives the corresponding calculation formula of the errors.

$$\begin{cases} e_{u_{dc}} = u_{dc_{ref}} - u_{dc} \\ e_{i_q} = i_{q_{ref}} - i_q \\ e_{\phi} = \phi_{ref} - \phi \end{cases} \tag{9}$$

In order to obtain better control performance, the independent variables of sliding mode surface function are usually selected as the deviations of system state variables. In this paper, corresponding to U_{dc} and i_q, respectively, two sliding surfaces s_1 and s_2 are created as

$$\begin{cases} s_1(e_{i_q}, t) = \sigma(i_{q_{ref}} - i_q) = 0 \\ s_2(e_{U_{dc}}, e_{\phi}, t) = \sigma_1(U_{dc_{ref}} - u_{dc}) + \sigma_2(\phi_{ref} - \phi) = 0 \end{cases} \tag{10}$$

In (10), σ, σ_1 and σ_2 are the amplification gains. Reasonable selection of the amplification gains can keep the system running steadily with fast dynamic response. Simplifying the second equation of (10), we can obtain

$$s_2(e_{u_{dc}}, e_{\phi}, t) = (U_{dc_{ref}} - U_{dc}) + \frac{\sigma_2}{\sigma_1}(\phi_{ref} - \phi) = e_{U_{dc}} + \lambda e_{\phi} = 0 \tag{11}$$

where λ is the time constant related to the first-order response of the output voltage U_{dc}. In other words, λ is the feedback coefficient of SMC. The smaller λ is, the faster the dynamic response is. However, considering the dead time and the delay of the switching device, λ cannot be designed too small, otherwise it is not conducive to reducing chattering. In addition, $(e_{udc}, e_{\varphi}, t) = 0$ in (10) represents a first-order filter, then the feedback coefficient λ can be regarded as the inverse of the cut-off frequency of this filter.

According to (9), (11) can be rewritten as

$$\begin{aligned} s_2(e_{U_{dc}}, e_{\phi}, t) &= e_{U_{dc}} + \lambda e_{\phi} \\ &= (U_{dc_{ref}} - U_{dc}) + \lambda(\phi_{ref} - \phi) \\ &= (U_{dc_{ref}} - U_{dc}) + \lambda\left(\frac{dU_{dc_{ref}}}{dt} - \frac{dU_{dc}}{dt}\right) \end{aligned} \tag{12}$$

From (3), we can obtain

$$\frac{dU_{dc}}{dt} = \frac{1}{C} i_{dc} - \frac{1}{C}\left(\begin{array}{l} \frac{3m^2 U_{dc}}{8}\sqrt{\frac{1+\rho^2 - 2\rho\cos\theta}{R^2 + (\omega L)^2}} \\ \cdot\left[\cos(\theta+\gamma) - e^{-t/\tau}\cos(\omega t + \theta + \gamma)\right] \end{array}\right) \tag{13}$$

U_{dcref} is a given constant, so $dU_{dcref}/dt = 0$. Hence, (12) can be rewritten as

$$\begin{aligned} & s_2(e_{u_{dc}}, e_{\phi}, t) \\ & = (U_{dc_{ref}} - U_{dc}) \\ & \quad -\lambda\left[\frac{S_d}{C} i_d + \frac{S_q}{C} i_q - \frac{1}{C}\left(\begin{array}{l} \frac{3m^2 U_{dc}}{8}\sqrt{\frac{1+\rho^2 - 2\rho\cos\theta}{R^2 + (\omega L)^2}} \\ \cdot\left[\cos(\theta+\gamma) - e^{-t/\tau}\cos(\omega t + \theta + \gamma)\right] \end{array}\right)\right] \end{aligned} \tag{14}$$

Extracting i_d in (14), we can obtain

$$\underbrace{\frac{C}{\lambda S_d}\left[\begin{array}{l} (U_{dc_{ref}} - U_{dc}) - \lambda\frac{S_q i_q}{C} + \frac{3\lambda m^2 U_{dc}}{8C}\sqrt{\frac{1+\rho^2 - 2\rho\cos\theta}{R^2 + (\omega L)^2}} \\ \cdot\left[\cos(\theta+\gamma) - e^{-t/\tau}\cos(\omega t + \theta + \gamma)\right] \end{array}\right]}_{i_{dref}} - i_d = 0 \tag{15}$$

where U_{dc} and i_q are measured.

According to (15), i_{dref} can be obtained. According to the principle of coordinate transformation power balance, the expression of the switching function S_d can be derived as

$$S_d = \frac{e_d - R i_d}{U_{dc}} \tag{16}$$

From (7), we can obtain

$$\frac{di_q}{dt} = -\frac{R_n}{L_n} i_q + \omega i_d + \frac{1}{L_n} e_q - \frac{1}{L_n} S_q U_{dc} \tag{17}$$

The transformer in EMUs has a large capacity, so the resistance R_n can be neglected. Ideally, $di_q/dt = 0$ and $e_q = 0$, so the switching function S_q can be obtained as

$$S_q = \frac{\omega L i_d}{U_{dc}} \tag{18}$$

Substituting (16) and (18) into (15), we can obtain the expression of i_{dref}.

$$\begin{aligned} i_{d_{ref}} = & \frac{C}{\lambda} \times \frac{U_{dc}}{e_d - R_n i_d} \\ & \times \left[\begin{array}{l} (U_{dc_{ref}} - U_{dc}) + \frac{3\lambda m^2 U_{dc}}{8C}\sqrt{\frac{1+\rho^2 - 2\rho\cos\theta}{R^2 + (\omega L)^2}} \\ \cdot\left[\cos(\theta+\gamma) - e^{-t/\tau}\cos(\omega t + \theta + \gamma)\right] \end{array}\right] \end{aligned} \tag{19}$$

Fig. 5 shows the block diagram of voltage loop controller, which is built according to (19). The voltage loop controller provides the active current reference value for the current loop controller.

B. INNER LOOP CURRENT CONTROL

In this paper, the exponential control law is chosen, as shown in (20), which ensures the vehicle-grid system owns better dynamic and static performance. $-ks$ is an exponent term, which makes the system state quickly approach the sliding

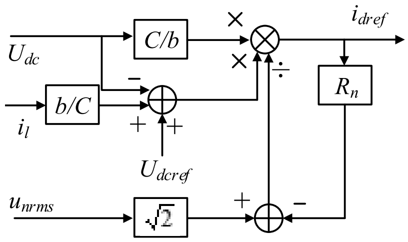

FIGURE 5. Block diagram of voltage loop controller.

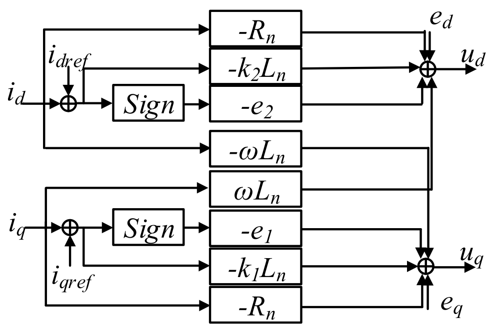

FIGURE 6. Block diagram of current loop controller.

mode surface when the system state is far away from the sliding mode surface; $-esgn(s)$ is a isokinetic approach term, which reduces the approach speed of the system state and avoid strong chatter when the system state is closer to the sliding mode surface. k and e are constants and they have a wide range of choices, that is, $600 \leq k \leq 1000$ and $e \leq 10^5$

$$\dot{s} = -e\mathrm{sgn}(s) - ks \quad (e > 0, k > 0) \tag{20}$$

Applying the exponential control law to the two sliding surfaces s_1 and s_2 in (10), we can obtain

$$\begin{cases} \dot{s}_1 = -e_1\mathrm{sgn}(s_1) - k_1 s_1 & (e_1 > 0, k_1 > 0) \\ \dot{s}_2 = -e_2\mathrm{sgn}(s_2) - k_2 s_2 & (e_2 > 0, k_2 > 0) \end{cases} \tag{21}$$

Substituting (21) into (9), the expression of the switch function can be obtained as

$$\begin{cases} S_q = \dfrac{e_q - R_n i_q - \omega L_n i_d - k_1 L_n s_1 - e_1\mathrm{sgn}(s_1)}{U_{dc}} \\ S_d = \dfrac{e_d - R_n i_d + \omega L_n i_q - k_2 L_n s_2 - e_2\mathrm{sgn}(s_2)}{U_{dc}} \end{cases} \tag{22}$$

Then the two electrical quantities input to the PWM module are obtained as

$$\begin{cases} u_q = S_q U_{dc} \\ u_d = S_d U_{dc} \end{cases} \tag{23}$$

Fig. 6 shows the block diagram of current loop controller, which is built according to (22) and (23). Based on the Park transformation, the rotating electrical quantities in (23) can be converted into static electrical quantities. Hence, the switch signals in α-β frame can be obtained.

TABLE 1. Simulation parameters of EMUs.

System Parameters	Value	Control Parameters	Value
$U_s(V)$	27500	K_p	100
$C(F)$	0.005	K_i	10
$U_{dc_{ref}}(V)$	3000	$T_{\lim}(N\cdot m)$	2000
$R_n(\Omega)$	0.145	K_{vp}	0.5
$L_n(H)$	0.0023	K_{vi}	1
$L_2(H)$	0.00084	K_{ip}	4
$C_2(F)$	0.003	$k_i(i=1,2)$	800
$T_s(s)$	0.00005	$e_i(i=1,2)$	0.1
-	-	λ	9e-3
-	-	$f_1(Hz)$	350
-	-	$f_2(Hz)$	500

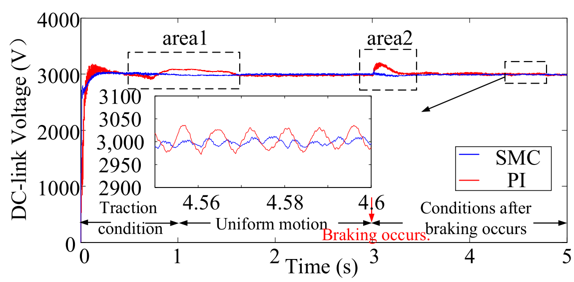

FIGURE 7. DC-side voltage of EMUs LSC under multiple operating conditions.

IV. THE SIMULATION COMPARISON OF CONTROL PERFORMANCE

The simulation models of EMUs based on SMC and PI control are built in Matlab/Simulink, respectively. The motors adopt indirect rotator field-orientation vector control strategy [17], [18]. The key parameters of the simulation model are shown in Table 1. T_s is sampling time. f_1 and f_2 are the switching frequencies of the rectifier and converter, respectively. K_p and K_i are the PI parameters of speed regulator in the inverter. T_{lim} is the limit value of the motor torque. K_{vp} and K_{vi} are the PI parameters of the voltage loop, K_{ip} is the proportional parameter of the current loop. In this Section, the performance based on PI control and SMC is compared.

A. COMPARISON OF CONTROL PERFORMANCE IN ONE TRACTION DRIVE UNIT OF EMUs UNDER MULTIPLE OPERATING CONDITIONS

1) THE WAVEFORMS OF U_{dc} WHEN ONE TRACTION DRIVE UNIT OF EMUs RUNS UNDER MULTIPLE OPERATING CONDITIONS

Through setting the given speed of the motor at different values, the EMU can run in different conditions. Fig. 7 shows the simulation waveforms of the one traction drive unit of EMUs under SMC and PI control. The EMU runs in the

TABLE 2. Performance indexes of DC-link voltage under traction.

Control strategy	Overshoot (%)	Peak time(s)	Response time(s)
PI	6.07	0.12	0.36
SMC	-	-	0.188

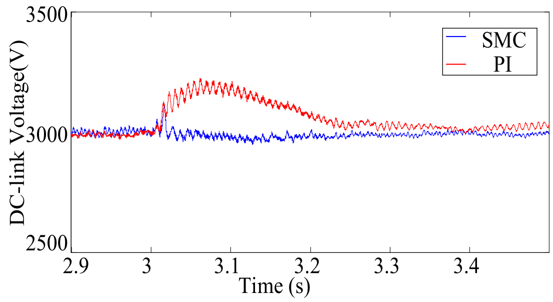

FIGURE 8. Magnified waveform of U_{dc} in area 2.

TABLE 3. Performance indexes of EMUs under braking condition.

Control strategy	Voltage fluctuation (V)	Peak valley (V)	Response time(s)
PI	36	3223	0.243
SMC	12	3119	0.018

traction state at 0-3s and regenerative braking occurs at 3s. Specific comparison results are given in Table 2. As can be seen, the control performance of SMC is better than that of PI control. The waveform of U_{dc} based on SMC has no overshoot, but the overshoot based on PI control is 6.07%. The response time for PI control is 0.36 s, whereas that for SMC is only 0.188s.

As shown in the area1 in Fig. 7, when the motor operation mode transits from traction to uniform motion, U_{dc} under PI control decreases at first and then increases. The reason is that when the EMU runs in traction condition, the EMU absorbs power from the grid side, and the input energy of the rectifier is smaller than the output energy, which causes a drop in U_{dc}. When the EMU operates in uniform motion state, the output power of the rectifier decreases rapidly, which causes a rise in U_{dc}. In essence, under PI control, the power of the rectifier cannot match the inverter well. However, with SMC, the fluctuation of U_{dc} is decreased obviously.

Moreover, as shown in area 2 in Fig. 7, under PI control, there is a large voltage fluctuation in U_{dc} as braking occurs, the enlarged view of which is shown in Fig. 8. The specific comparison results are listed in Table 3. As can be seen, the peak valley of U_{dc} is 3223V under PI control, whereas that under SMC is 3119V. U_{dc} returns to 3000V at 0.018s when SMC is adopted. However, the response time under PI control is 0.243s. Besides, the voltage fluctuation in stable state under PI control is 36V, whereas that under SMC is only 12V.

2) THD OF GRID-SIDE CURRENT UNDER MULTIPLE OPERATING CONDITIONS

When the EMU runs under different conditions, the THD of the grid-side current of EMU is also different. When the EMU runs under traction condition or braking condition, the THD

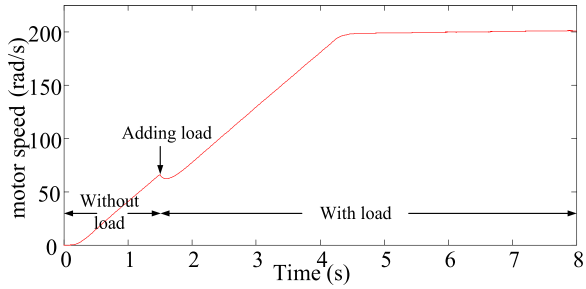

FIGURE 9. Motor speed w_r under traction condition and uniform motion based on SMC.

of grid-side current increases [19]. Fig. 9 shows the waveform of motor speed ω_r based on SMC. At 1.5s, a 1500N.m load is added. At 0-4.2s, the EMU runs in traction condition. When the ω_r reaches 200 rad/s, the EMU runs in uniform motion condition.

Fig. 10 shows the waveforms and THD of the grid-side current i_s at 3.3-3.5s when the EMU runs under traction condition based on SMC and PI control. It can be concluded that when the EMU runs in traction condition, the waveform of the grid-side current under SMC is more similar to sine wave, and the THD is 26.59%, which is lower than that under PI control. Therefore, the THD in traction condition can be effectively reduced with SMC.

Fig. 11 shows the waveforms and THD of the grid-side current i_s at 4.4-4.6s when the EMU runs at a constant speed based on SMC and PI control. The waveform of i_s under SMC is closer to the sine wave, and the THD is 22.42%, which is lower than that under PI control. Therefore, SMC can also reduce the THD when the EMU runs at a constant speed.

Fig. 12 shows the waveforms of motor speed ω_r under multiple operating conditions based on SMC. The given speed is set to 200 rad/s at 0s and 0 rad/s at 3s. The load torque (1500N.m) is added at 1.5s. As can be seen, ω_r rises from 0 rad/s to 210 rad/s during 0-1.5s. After the load is added, ω_r drops from 210 rad/s to 200 rad/s and maintains at a constant. ω_r starts to decrease at 3s and drops to 0 at around 3.6s.

Fig. 13 shows the active power and reactive power in grid when SMC is adopted in LSC. It can be seen that, at 3s, the active power changes from a positive value to a negative value, which indicates that the energy is fed back to the grid by the motors. That is to say, the regenerative braking occurs at 3s. The reactive power is always kept at zero, so the EMU absorbs almost no reactive power from the grid.

Fig. 14 shows the waveforms and THD of the grid-side current at 3.1-3.3s when EMU runs under braking condition based on SMC and PI control. The THD under SMC is 32.14%, which is lower than that under PI control. Therefore, the SMC can also reduce the THD under the braking condition.

B. ANTI-INTERFERENCE ABILITY COMPARISON IN MULTI-EMUs SYSTEM

In order to study the anti-interference ability of the system with SMC and PI control when the equivalent inductance

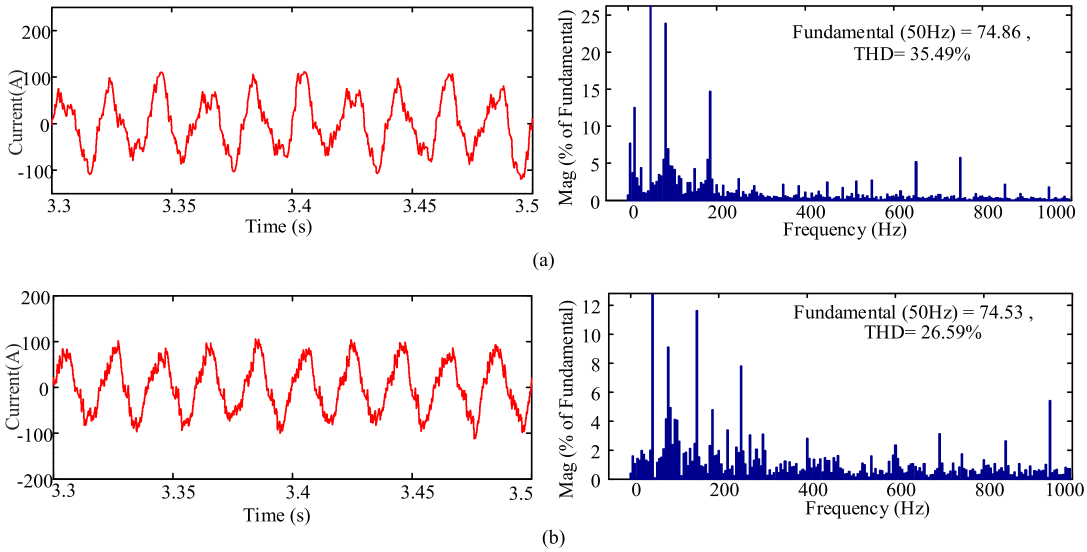

FIGURE 10. **Line-side current waveform and its THD in traction condition based on (a) PI control (b) SMC.**

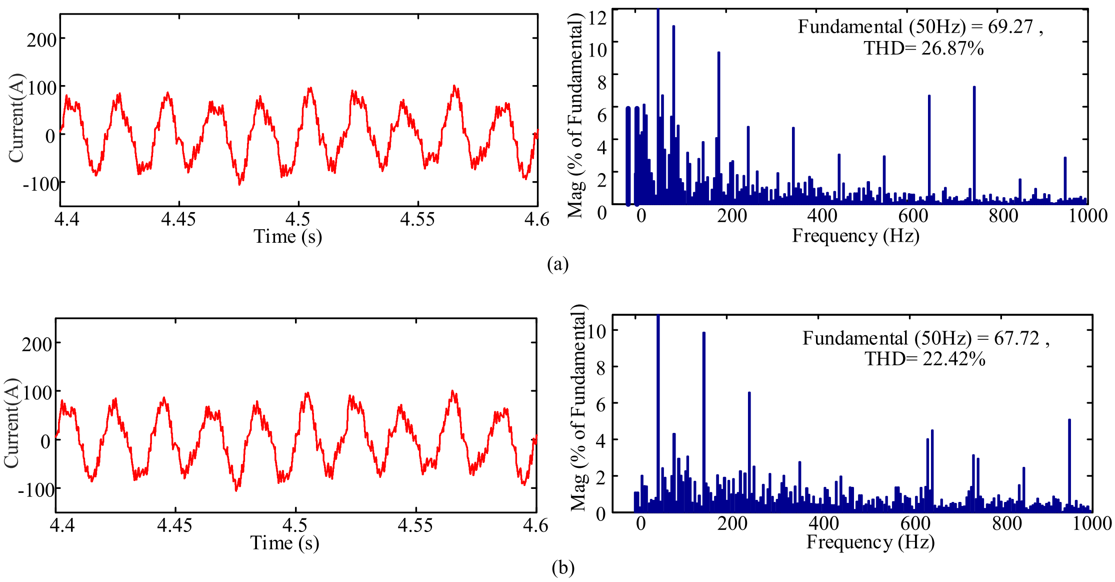

FIGURE 11. **Grid-side current waveform and its THD under constant speed operation condition based on (a) PI control (b) SMC.**

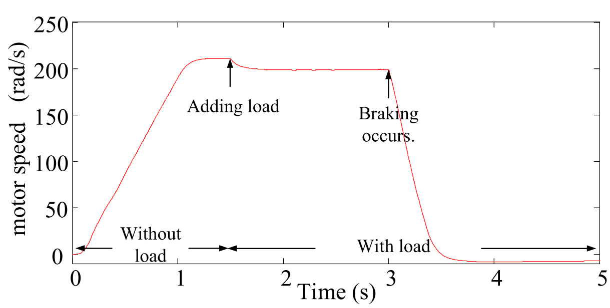

FIGURE 12. **Motor speed w_r under multiple operating conditions based on SMC.**

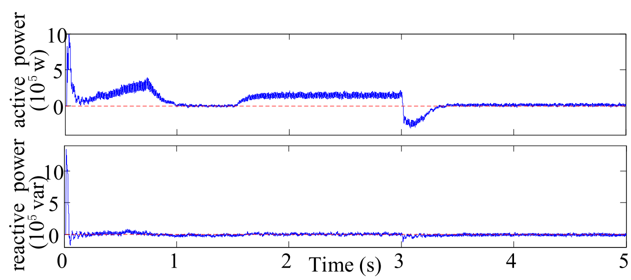

FIGURE 13. **Grid-side active and reactive power with SMC.**

of the vehicle-side L_n changes, this paper builds a multi-vehicle cascade system, as shown in Fig. 15, where $n = 2$. All of the EMUs are connected to the traction network at 0s.

R_s and L_s are grid-side equivalent inductance and resistance, respectively.

Fig. 16 shows the waveforms of U_{dc} under PI control when L_n is set as 0.003, 0.005 and 0.009, respectively, where the

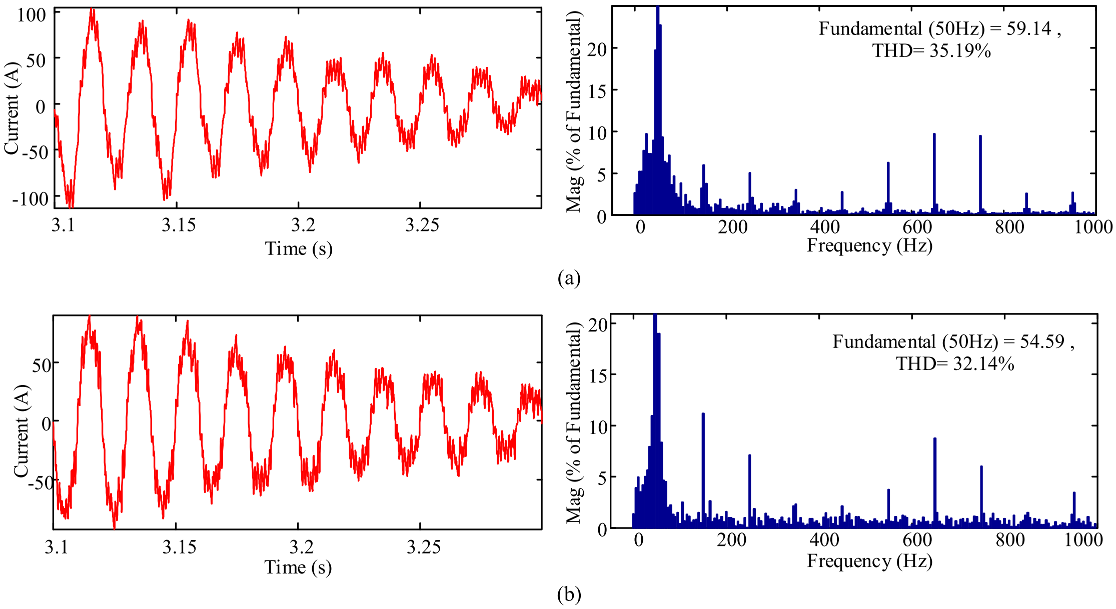

FIGURE 14. Line-side current waveform and its THD under braking condition based on (a) PI control (b) SMC.

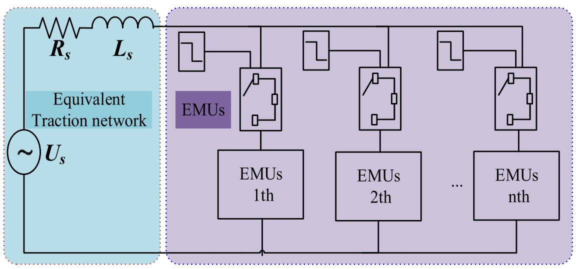

FIGURE 15. The simplified vehicle-grid system.

TABLE 4. Main system parameters in simplified vehicle-grid system.

Parameters	Value
$R_s(\Omega)$	0.145
$L_s(H)$	0.005
$R_n(\Omega)$	0.145
$L_n(H)$	0.0023

waveforms at 3s to 4s are amplified. We can see that when L_n is increased, the deviation of U_{dc} becomes larger.

Fig. 17 shows the waveforms of U_{dc} based on SMC when L_n is set as 0.003, 0.005, and 0.009, respectively. Similarly, the waveforms at 3-4s are amplified. We can see that, with different L_n, the deviation of U_{dc} is basically the same, which is $\pm$20V. Therefore, the system with SMC is less sensitive to the change of L_n. That is to say, SMC has better anti-reference ability.

C. SUPRESSION OF LFO DURING MULTIPLE OPERATION CONDITIONS WITH SMC IN MULTI-EMUs SYSTEM

In order to verify the LFO suppression effect of SMC under different operation conditions, this paper analyzes the

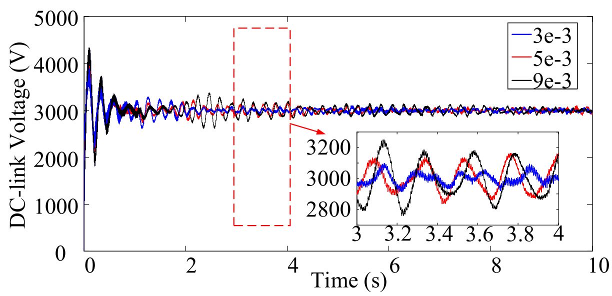

FIGURE 16. Waveforms of the electrical quantities of EMUs when L_n changes with PI control.

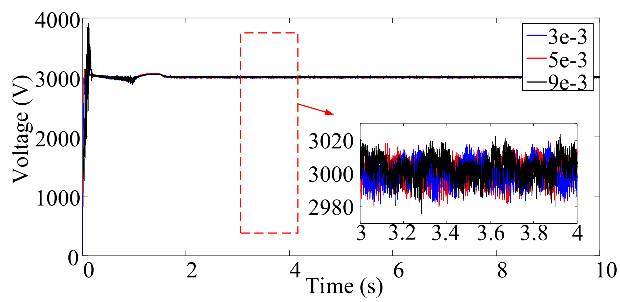

FIGURE 17. Waveforms of the electrical quantities of EMUs when L_n changes with SMC.

performance of u_n, i_n, and U_{dc} based on SMC and PI control when EMUs run in traction condition, uniform motion condition and braking condition, respectively. The change of the given speed is the same as that in Fig. 12.

1) CONTROL PERFORMANCE BASED ON PI CONTROL

Fig. 18 show the waveforms of the u_n, i_n, and U_{dc} based on PI control when L_s is set to 0.03H. Area 1 and area 2 present the

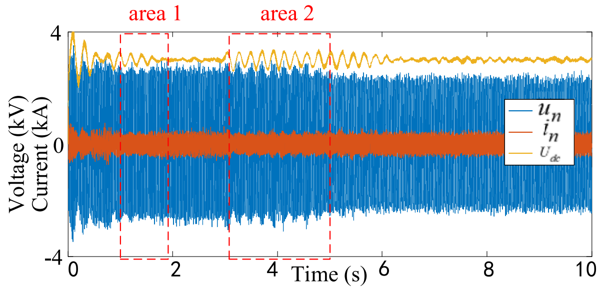

FIGURE 18. Waveforms of u_n, i_n, and U_{dc} when LFO occurs under PI control.

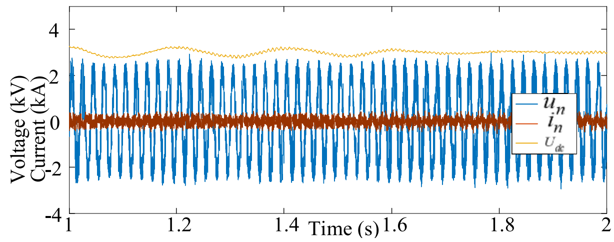

FIGURE 19. Magnified waveforms of u_n, i_n, and U_{dc} in area 1.

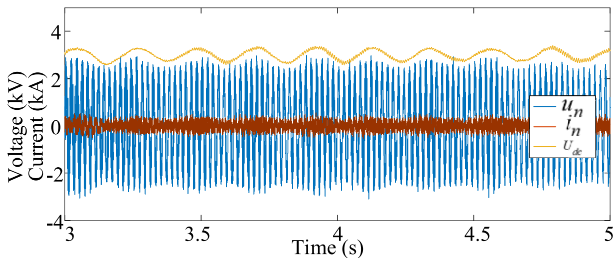

FIGURE 20. Magnified waveforms of u_n, i_n, and U_{dc} in area 2.

waveforms when EMUs run under uniform motion condition and regenerative braking condition, respectively. Because of the mismatch between the parameters of the traction network and the control parameters of LSC, the LFO occurs in the two areas.

Fig. 19 shows the amplified area 1. Before ω_r rises to the given speed, the EMUs violently oscillate. When ω_r stabilizes, the fluctuation of the electrical quantities becomes smaller, and the oscillation frequency is 5Hz. u_n and U_{dc} oscillates in synchronization. Fig. 20 shows the amplified waveforms of area 2. The fluctuation range of U_{dc} is increased compared with that during 2-3s. The oscillation frequency is still 5Hz, and u_n still oscillates in synchronization with U_{dc}.

2) CONTROL PERFORMANCE BASED ON SMC

It can be seen from the Fig. 21 that when the LSC adopts SMC, U_{dc} can be stabilized at 3000V. There is no oscillation in U_{dc} and u_n. For U_{dc}, there is also no overshoot when EMUs are powered at 0s and less fluctuation when braking occurs at 3s. It should be noted that the fluctuation of U_{dc} in Fig. 21 is larger than that in Fig. 8 at the motor braking state, which

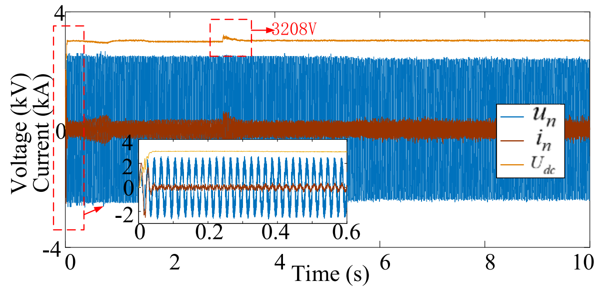

FIGURE 21. Waveforms of u_n, i_n, and U_{dc} when the vehicle-grid system adopts SMC.

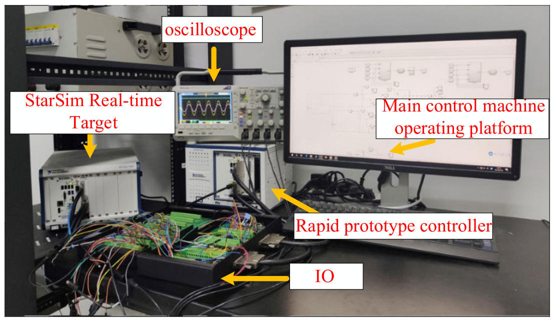

FIGURE 22. Semi-physical test platform.

is caused by the worse operation condition in Fig. 21 where multi-EMUs operates at the same time. Therefore, SMC can effectively suppress the LFO when the EMUs operate under multiple conditions.

V. SEMI-PHYSICAL VERIFICATION OF VEHICLE-GRID SYSTEM

In order to further verify that the control performance of SMC is better than that of PI control, in this paper, the experiments are conducted in the HIL platform, whose schematic diagram is shown in Fig. 22.

The main circuit model of EMU is developed in the electromagnetic transient simulation software StarSim and runs on the real-time HIL system based on NI-PXIe-FPGA-7868R. The control algorithm of EMU runs on the CPU. The IO board contains a number of IO channels that can make the electrical quantities, such as the voltage, current, motor speed, and electromagnetic torque, transmitted to the oscilloscope for observation. The parameters of the entire system are shown in the Table 1.

A. EXPERIMENTAL RESULTS OF ELECTRICAL QUANTITIES ON THE AC-SIDE OF THE INVERTER BASED ON SMC

In Fig. 23, i_a, i_b and i_c are three-phase symmetrical sinusoidal currents at the stator side. T_{em} is the electromagnetic torque of the motor. When the EMU is powered, T_{em} and ω_r both rise from zero. Before ω_r rises to the given speed, there is a certain fluctuation in T_{em}. After ω_r reaches 200 rad/s, T_{em} drops to zero. i_a, i_b and i_c is reduced from 400A to 200A. At 1.5s, a 1000N.m load is added, so T_{em} rises rapidly to 1000N.m to

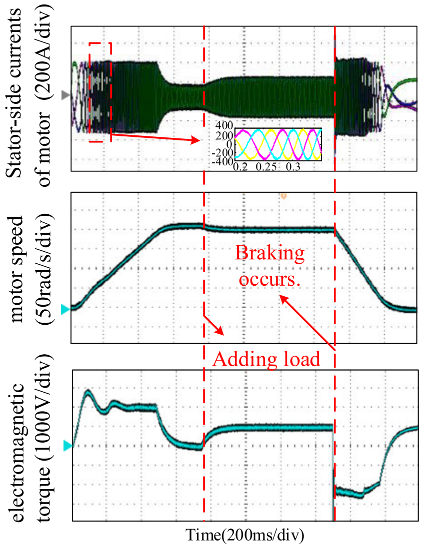

FIGURE 23. Waveforms of electrical quantities on the AC-side of the inverter based on SMC.

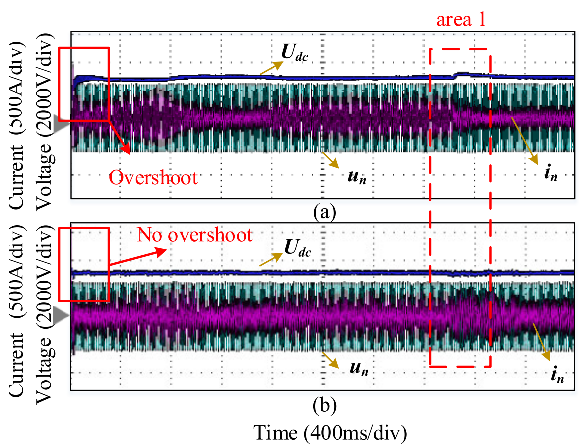

FIGURE 24. Waveforms of u_n, i_n, and U_{dc} under different controllers. (a) PI control. (b) SMC.

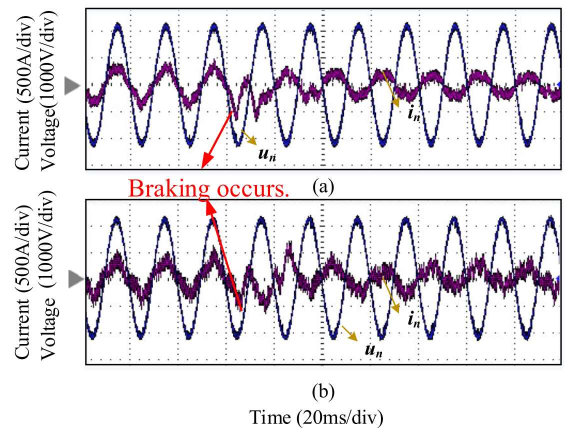

FIGURE 25. Waveforms of u_n, i_n, and U_{dc} under (a) PI control. (b) SMC in braking condition.

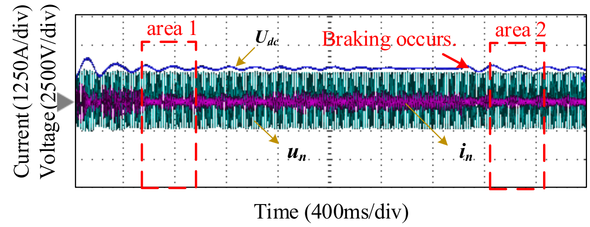

FIGURE 26. Waveforms of u_n, i_n, and U_{dc} based on PI control in multi-EMUs.

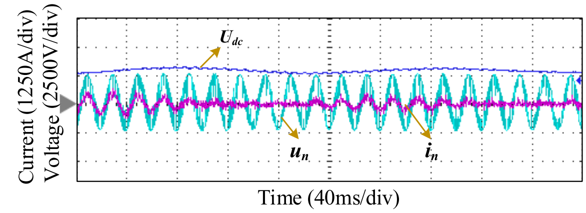

FIGURE 27. Magnified waveforms of u_n, i_n, and U_{dc} in area 1.

balance with the load torque. At 3s, the regenerative braking occurs in the EMUs and ω_r starts to drop. T_{em} turns to -2500 N·m, and the motor becomes a generator, which feeds the energy back to the grid. Until ω_r drops to 0, T_{em} rises to the load torque.

B. EXPERIMENTAL RESULTS OF u_n, i_n, AND U_{dc} BASED ON SMC AND PI CONTROL WHEN ONE TRACTION DRIVE UNIT OF EMUs RUNS UNDER MULTI-OPERATING CONDITIONS

Fig. 24 shows the waveforms of u_n, i_n, and U_{dc} under multiple conditions. As can be seen, there is a certain overshoot when the EMU under PI control is powered. However, when SMC is adopted, the overshoot is eliminated. When regenerative braking occurs in EMU, the DC-side voltage fluctuation under PI control is larger than that under SMC. The experimental results verify that the DC-side voltage based on SMC is more stable than that under PI control when the EMU runs under the traction condition and the braking condition.

Fig. 25 shows the magnified view of area 1 in Fig. 24, where the regenerative braking occurs. As can be seen, the phase of u_n and i_n quickly change from the same values to the opposite values, which indicates that SMC and PI control both can achieve a smooth transition of electrical quantities when system operation condition is changed.

The experiment results are consistent with the simulated results, which can verify the correctness of simulated results in Section IV.

C. EXPERIMENTAL RESULTS OF u_n, i_n, AND U_{dc} BASED ON SMC AND PI CONTROL WHEN MULTI-EMUs RUN UNDER MULTI-OPERATING CONDITIONS

As shown in Fig. 26, when multi-EMUs with PI control are accessed to the traction network, LFO occurs. Area1 and area2 present the waveforms when multi-EMUs run under

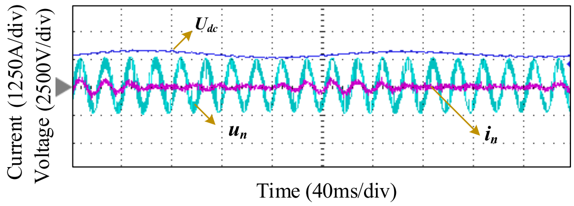

FIGURE 28. Magnified waveforms of u_n, i_n, and U_{dc} in area 2.

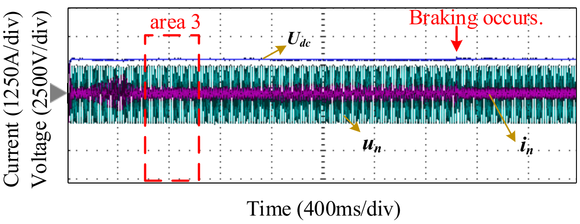

FIGURE 29. Waveforms of u_n, i_n, and U_{dc} based on SMC in multi-EMUs.

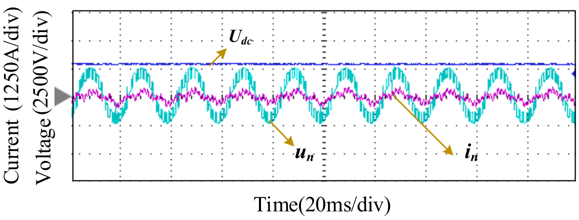

FIGURE 30. Magnified waveforms of u_n, i_n, and U_{dc} in area 3.

traction and braking conditions, respectively. The magnified waveforms of area1 and area2 are shown in Fig. 27 and Fig. 28, respectively. It can be seen that u_n, i_n, and U_{dc} all oscillate at the same frequency.

When SMC is adopted to the LSCs of multi-EMUs, the LFO of u_n, i_n, and U_{dc} is suppressed, as shown in Fig. 29. The magnified waveforms of area3 are shown in Fig. 30. As can be seen, the amplitude of U_{dc} is kept at 3000V, and there is no oscillation in u_n and i_n. Therefore, we can obtain the conclusion that SMC can suppress the LFO occurs in multi-operating conditions.

VI. CONCLUSION

To improve the performance of EMUs under multiple operating conditions, SMC is proposed in this paper. According to the simulation and experiment results, the following conclusions can be drawn.

1) Compared with PI control, SMC has a better dynamic performance and faster dynamic response under multiple operation conditions, such as no overshoot when the motors are powered, and better anti-interference ability when the motors brake.

2) SMC can make the waveform of the grid-side current closer to sine wave. The THD of grid-side current under SMC is smaller than that under PI control when the EMU runs under traction, braking and uniform motion conditions, respectively.

3) Based on SMC, the system is less sensitive to system parameters, which means SMC has stronger robustness than PI control.

4) SMC can effectively suppress the LFO that occurs under multiple operation conditions.

However, SMC has some disadvantages. For example, when the load torque of the motor changes or the grid voltage changes, the DC-side voltage of the LSC cannot follow the given value. Future work can aim at overcoming these shortcomings. The SMC can be combined with state observers, so that the system dynamic performance, static performance and robustness can be further improved.

REFERENCES

[1] H. Cui, X. Feng, X. Lin, and Q. Wang, "Research on harmonic resonance characteristic of high-speed railway traction net considering coupling of trains and traction nets," *Trans. China Electrotech. Soc.*, vol. 28, no. 9, pp. 54–64, Sep. 2013.

[2] J. Wang, Y. Qi, and S. Li, "Analysis and simulation of harmonic current in the grid-side converter of AC-DC-AC locomotive," *High Power Converter Technol.*, no. 3, pp. 12–16, Jun. 2016.

[3] C. Liu, "Study on harmonic characteristics of Baoshen railway Shenhua electric locomotive," *Electr. Railway*, vol. 29, no. 4, pp. 19–24, Aug. 2018.

[4] S. Danielsen, O. B. Fosso, M. Molinas, J. A. Suul, and T. Toftevaag, "Simplified models of a single-phase power electronic inverter for railway power system stability analysis—Development and evaluation," *Electr. Power Syst. Res.*, vol. 80, no. 2, pp. 204–214, Feb. 2010.

[5] X. Zhang, J. Chen, G. Zhang, L. Wang, R. Qiu, and Z. Liu, "An active oscillation compensation method to mitigate high-frequency harmonic instability and low-frequency oscillation in railway traction power supply system," *IEEE Access*, vol. 6, pp. 70359–70367, 2018.

[6] H. Hu, H. Tao, F. Blaabjerg, X. Wang, Z. He, and S. Gao, "Train–network interactions and stability evaluation in high-speed Railways—Part I: Phenomena and modeling," *IEEE Trans. Power Electron.*, vol. 33, no. 6, pp. 4627–4642, Jun. 2018.

[7] J. Liu, T. Q. Zheng, and Q. Yang, "Resonance mechanism between traction drive system of high-speed train and traction network," *Trans. China Electrotech. Soc.*, vol. 28, no. 4, pp. 221–227, Apr. 2013.

[8] Z. Liu, X. Hu, and Y. Liao, "Vehicle-grid system stability analysis based on norm criterion and suppression of low-frequency oscillation with MMC-STATCOM," *IEEE Trans. Transp. Electrific.*, vol. 4, no. 3, pp. 757–766, Sep. 2018.

[9] H. Wang, W. Mingli, and J. Sun, "Analysis of low-frequency oscillation in electric railways based on small-signal modeling of vehicle-grid system in DQ frame," *IEEE Trans. Power Electron.*, vol. 30, no. 9, pp. 5318–5330, Sep. 2015.

[10] Y. Liao, Z. Liu, G. Zhang, and C. Xiang, "Vehicle-grid system modeling and stability analysis with forbidden region-based criterion," *IEEE Trans. Power Electron.*, vol. 32, no. 5, pp. 3499–3512, May 2017.

[11] Z. Liu, S. Liu, Z. Li, and I. A. Tasiu, "A novel approach based on extended state observer sliding mode control to suppress voltage low frequency oscillation of traction network," *IEEE Access*, vol. 7, pp. 52440–52454, 2019.

[12] Z. Liu, Y. Wang, S. Liu, Z. Li, H. Zhang, and Z. Zhang, "An approach to suppress low-frequency oscillation by combining extended state observer with model predictive control of EMUs rectifier," *IEEE Trans. Power Electron.*, vol. 34, no. 10, pp. 10282–10297, Oct. 2019.

[13] Z. Geng, Z. Liu, X. Hu, and J. Liu, "Low-frequency oscillation suppression of the vehicle–grid system in high-speed railways based on H_∞ control," *Energies*, vol. 11, no. 6, p. 1594, Jun. 2018.

[14] C. Heising, R. Bartelt, M. Oettmeier, V. Staudt, and A. Steimel, "Improvement of low-frequency system stability in 50-Hz railway-power grids by multivariable line-converter control in a distance-variation scenario," in *Proc. Electr. Syst. for Aircraft, Railway Ship Propuls.*, Oct. 2010, pp. 1–5.

[15] H. Wang and M. Wu, "Review of low-frequency oscillation in electric railways," *Trans. China Electrotech. Soc.*, vol. 30, pp. 70–78, Sep. 2015.

[16] Z. Jiasheng and Z. Lei, "Research on the DC-side equivalent model of PWM inverters," *Proc. CSEE*, vol. 32, no. 5, pp. 1130–1138, Feb. 2007.

[17] F. Xiaoyun, W. Lijun, G. Xinglai, and L. Guanjun, "Research and simulation on traction and drive control system of high-speed EMU," *Electr. Drive*, no. 11, pp. 25–28, Nov. 2008.
[18] D. Juxia and J. Kui, "Research and simulation on three modulation strategies of traction inverter in CRH3 EMU," *Electr. Drive*, vol. 44, no. 6, pp. 46–49, Jun. 2014.
[19] L. Dapeng, "Load harmonic analysis and simulation research based on different operation conditions of electric locomotive," *Silicon Valley*, vol. 7, no. 9, pp. 52–53, May 2014.

YUTING ZHANG received the B.S. degree in automation from East China Jiaotong University, Nanchang, China, in 2018. She is currently pursuing the master's degree with the School of Electrical Engineering, Southwest Jiaotong University. Her research interest includes the improvement of the vehicle-grid system performance under multiple operating conditions.

SIQI WU (Student Member, IEEE) received the B.S. degree in electrical engineering and its automation from Huaqiao University, Xiamen, China, in 2016. She is currently pursuing the Ph.D. degree with the School of Electrical Engineering, Southwest Jiaotong University, Chengdu, China. Her research interest includes the modeling and stability analysis of power electronics-based systems.

ZHIGANG LIU (Senior Member, IEEE) received the Ph.D. degree in power system and its automation from the Southwest Jiaotong University, China, in 2003.

He is currently a Full Professor with the School of Electrical Engineering, Southwest Jiaotong University. He has written three books, published more than 100 peer-reviewed journal articles and conference papers. His research interests are the electrical relationship of EMUs and traction, detection and assessment of pantograph-catenary in high-speed railway. He was elected as a fellow of the Institution of Engineering and Technology (IET), in 2017. He received the IEEE TIM's Outstanding Associate Editors for 2019 and the Outstanding Reviewer of the IEEE Transactions on Instrumentation and Measurement, in 2018. He is an Associate Editor of the IEEE Transactions on Neural Networks and Learning Systems, the IEEE Transactions on Vehicular Technology, the IEEE Transactions on Instrumentation and Measurement, and IEEE Access.

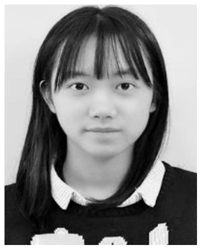

QIXIANG YAN received the B.S. degree in automation from the Changchun University of Science and Technology, Changchun, China, in 2018. She is currently pursuing the master's degree with the School of Electrical Engineering, Southwest Jiaotong University. Her research interest includes control methods of the vehicle-grid systems.

TAO CHEN received the B.S. degree in automation from East China Jiaotong University, Nanchang, China, in 2017. He is currently pursuing the master's degree with the School of Electrical Engineering, Southwest Jiaotong University. His research interest includes fault diagnosis and fault tolerance control of high-speed train converter.